Biotechnology and Bioengineering

WILEY

BIOTECHNOLOGY AND BIOENGINEERING

ARTICLE OPEN ACCESS

Expanding Metabolic Online Monitoring Capabilities in 96-Deepwell Microtiter Plates by Combining Optoelectronic O_2 and CO_2 Sensors

Robert Dinger[1] | David Pfeifer[2] | David Flitsch[3] | Jan P. Fischer[3] | Clemens Lattermann[4] | Sergey M. Borisov[2] | Jochen Büchs[1]

[1]Chair of Biochemical Engineering (AVT.BioVT), RWTH Aachen University, Aachen, North Rhine Westphalia, Germany | [2]Institute of Analytical Chemistry and Food Chemistry, Graz University of Technology, Graz, Styria, Austria | [3]PyroScience GmbH, Aachen, North Rhine Westphalia, Germany | [4]Kuhner Shaker GmbH, Herzogenrath, North Rhine Westphalia, Germany

Correspondence: Jochen Büchs (jochen.buechs@avt.rwth-aachen.de)

Received: 21 February 2026 | **Revised:** 4 July 2026 | **Accepted:** 17 July 2026

Funding: German Federal Ministry of Education and Research, Grant/Award Number: 031B0102A

Keywords: carbon dioxide transfer rate (CTR) | high-throughput | microtiter plate (MTP) | process monitoring | respiration activity

ABSTRACT

To increase the information content in early stages of bioprocess development, various technologies have been introduced for monitoring cultivations in microtiter plates (MTPs). Besides spectroscopical measurements, like in the BioLector technology, optical measurements with luminescent sensors, placed directly in the cultivation medium, became widely established. Monitoring the oxygen transfer rate (OTR) is a key technology for bioprocess development, as it allows mass balancing. At the same time, it is a criterion for a rational scale-up of cultivations. Although this technology has recently been transferred to monitoring of OTR in 96-well MTPs, monitoring of other parameters like carbon dioxide transfer rate (CTR) in individual wells was so far impossible. In this study, the preparation and integration of novel CO_2-sensitive fluorescent sensors into the micro (μ)-scale Transfer rate Online Measurement device (μTOM) is reported, that rely on spectrally compatible diketopyrrolopyrrole indicator dye. By including 48 CO_2 and 48 O_2 sensors, the 96-well sensor layout of the μTOM allows for simultaneous measurement of CTR and OTR in separate replicate wells and the calculation of 48 respiratory quotients (RQs). Additionally, to reduce the overall media consumption, liquid filling volumes between 0.2 and 0.5 mL were applied. The first-ever parallel monitoring of the OTR, CTR, and RQ in one MTP during cultivations of *Hansenula polymorpha* RB11 pC10-FMD (P_{FMD}-GFP) and *E. coli* BL21(DE3) pRotHi-YFP are presented. The interpretation of the RQ allowed distinguishing between the oxygen-unlimited growth of *Hansenula polymorpha* on glucose, as well as the accumulation and consumption of ethanol. Furthermore, the RQ was used to identify the sequential consumption of glucose and glycerol by *E. coli* BL21(DE3) in Wilms-MOPS autoinduction medium. Thus, the additional online parameters, CTR and RQ, extend the possibilities for early-stage bioprocess development at MTP-scale.

1 | Introduction

As state-of-the-art, screening experiments and early process development are performed in microbioreactors. Several case studies were published, showing the potential of microbioreactors in accelerating and cutting the costs of bioprocess development (Hemmerich et al. 2018; Lye et al. 2003). The success of micro-bioreactors is directly linked to novel analytical technologies, allowing for monitoring the performed cultivations. Besides online

spectroscopical measurements like in the BioLector technology (Kensy et al. 2009; Samorski et al. 2005), fluorescence sensor spot-based technologies are widely established for online monitoring. Typical parameters measured with sensor spots are, for example, dissolved oxygen tension (DOT), dissolved carbon dioxide (DCO_2), and pH. Broad overviews of established microbioreactor systems (Teworte et al. 2022) and applied optical sensor technologies have recently been published (Gruber et al. 2017).

The respiration activity is one of the most frequently measured parameters in all stages of bioprocess development. This parameter can directly be measured via off-gas analysis in the form of the oxygen transfer rate (OTR) and carbon dioxide transfer rate (CTR) or indirectly as the dissolved oxygen tension (DOT) in aqueous fermentation media. The respiration activity is directly correlated to biomass growth and product formation and is influenced by sub-optimal cultivation conditions, for example, pH-inhibition, substrate limitations, and oxygen limitation. Hence, the respiration activity is commonly used for process development and as a scale-up criterion (Anderlei et al. 2004; Müller et al. 2019).

From a combined measurement of the OTR and CTR, the apparent respiratory quotient (RQ = CTR/OTR) can be calculated. The RQ allows to characterize the metabolic activity of microorganisms with respect to the degree of reduction of the carbon source. Hence, diauxic growth on multiple substrates can be detected online. Furthermore, if the stoichiometry of the microbial metabolism is known, online identifying the consumed substrate is possible (Anderlei et al. 2004; M. J. Müller et al. 2018). In the case of oxygen-limited cultivation conditions, microorganisms like yeasts can switch to partially anaerobic metabolism, producing highly reduced by-products, such as ethanol (Stockmann et al. 2003) or 2,3-butandiol (Heyman et al. 2019). Under oxygen limitation, the measured OTR remains more or less constant. The formation of reduced by-products leads to increased RQ values > 1. Vice versa, the consumption of reduced by-products results in RQ values < 1 (Stockmann et al. 2003).

By reengineering the Respiration Activity Monitoring System (RAMOS) for shake flasks, Flitsch et al. (2016) were able to monitor the oxygen transfer rates in each well of 48-well microtiter plates (MTPs), using oxygen-sensitive sensor spots in the headspace of the wells (Flitsch et al. 2016). In 2022, Dinger et al. published the μTOM technology, allowing OTR measurements in 96-deepwell MTPs, using miniaturized optoelectronics (Dinger et al. 2022). However, compared to the RAMOS for shake flasks, the mentioned MTP systems lack the possibility to measure the CTR in parallel.

The optoelectronic sensor module of the μTOM measures the luminescence lifetime of the indicator dye contained in the sensor spot. The sensor spots are excited using LEDs emitting sinusoidal-modulated red light (610–630 nm) (Borisov et al. 2008). The emission of the sensor follows the excitation modulation. However, the emission is delayed due to the lifetime of the luminophore of the sensor. The delay is measured as the phase angle between the sinusoidal excitation and emission. In the case of the O_2-sensitive sensor spots applied in the μTOM device, the lifetimes of the luminophore significantly exceed 1 μs and can, therefore, be detected by miniaturized, and inexpensive instrumentation (Dinger et al. 2022; Lippitsch et al. 1988).

To establish the CO_2 measurement in the μTOM, a novel sensor system is required to meet the spectral requirements of the optoelectronics. Analogously to optical oxygen sensors, carbon dioxide concentrations can also be measured via luminescence (Liu et al. 2010; Mills and Chang 1993). However, these sensors utilize fluorescent pH indicators as transducers, that possess lifetimes in the nanosecond range. Unfortunately, these cannot be directly measured by the current setup of the μTOM device and require more sophisticated instrumentation, such as confocal laser scanning microscopes (Gruber et al. 2017). Moreover, many indicator dyes show "on"–"off" behavior, where a strong change in the luminescence intensity is not accompanied by any significant change in the decay time. In the μTOM device, CO_2 monitoring via phase angle measurements is possible by applying the dual lifetime referencing (DLR) method that has been described in detail in the literature (Huber et al. 2001). Briefly, apart from the fluorescent indicator, the composite material also contains an inert reference (typically, a metal-organic dye or an inorganic phosphor) with the luminescence decay in the microsecond time domain. The intensity of the sensing dye significantly changes in the presence of CO_2, whereas the reference material gives a constant signal. Consequently, the measured phase shift depends only on the ratio of intensities of the indicator and the reference material and thus, on the CO_2 concentration. Evidently, to enable CO_2 measurement in the μTOM device, it is essential to find a suitable "sensing chemistry" (i.e., the indicator dye and the reference material) that is spectrally compatible with the opto-electronics of the device. Advantageously, several reported fluorescent CO_2 indicators were demonstrated to be in principle compatible with the red-light excitation (Pfeifer et al. 2018; Rappitsch et al. 2020; Schutting et al. 2015). Also, robust inorganic phosphors, such as calcium copper silicate (Egyptian blue) (Borisov et al. 2013) and chromium(III)-activated gadolinium aluminum borate, show suitable spectral properties and thus, can be used as a reference in the DLR read-out scheme (Borisov et al. 2010). For this study, a new diketopyrrolopyrrole indicator (Supporting Information 1) has been synthesized. It relies on a biphenyl-substituted chromophore (Schutting et al. 2013), which is alkylated in one position with 4-tert-butyl-benzyl substituent similarly to the published compound (Schutting et al. 2014). The experimental details and analytical data are provided in the Supporting Information 1–3.

This work introduces preparation, integration, and calibration of the new CO_2-sensors in the μTOM device. With the integration of the novel combined O_2- and CO_2-sensor layout in the μTOM device, the first ever high throughput online measurement of RQs in 48 duplicate cultivations was established. Finally, combined OTR and CTR measurements in yeast and bacterial cultures are presented.

2 | Materials and Methods

2.1 | CO_2 Sensing Material

For this study, a new diketopyrrolopyrrole indicator (Supporting information 1) has been synthesized. It relies on a biphenyl-

substituted chromophore (Schutting et al. 2013), which is alkylated in one position with 4-tert-butyl-benzyl substituent similarly to the published compound (Schutting et al. 2014). The experimental details and analytical data are provided in the Supporting Information.

CO_2 sensing foil was prepared by dissolving/dispersing 0.5 mg of the indicator, 500 mg ethyl cellulose (49% ethoxyl), 12.5 µL of tributylphosphate, 20 µL tetraoctylammonium hydroxide (TOAOH, 20% wt solution in methanol), and 20 mg of Egyptian blue pigment in 900 mg of toluene:ethanol (3:2 v/v) mixture. This "cocktail" was knife-coated on a poly(ethylene terephthalate support) and after solvent evaporation, an additional protective layer (Fritzsche et al. 2017) composed of Hyflon AD 60 and Fomblin Y (9:1 w/w) was added.

2.2 | Microtiter Plates and Shake Flasks

All cultivations in the µTOM device (Dinger et al. 2022) were conducted in 96-deepwell MTP (Riplate RW, 2.0 mL round deepwell plate, HJ-BIOANALYTIK GmbH, Erkelenz, Germany). For sterility, the MTP was covered with a gas-permeable sealing film (AeraSeal™, Sigma-Aldrich Chemie GmbH, Taufkirchen, Germany).

All shake flask experiments were performed in modified 250 mL RAMOS shake flasks and monitored in an in-house built RAMOS device. The RAMOS technology for shake flasks is commercially available as TOM device from Kuhner AG (Birsfelden, Switzerland) or RAMOS from HiTec Zang GmbH (Herzogenrath, Germany).

For this study, two different microorganisms were cultivated: *E. coli* BL21(DE3) pRotHi-YFP and *Hansenula polymorpha* RB11 pC10-*FMD* (P_{FMD}-GFP).

2.3 | Media and Cultivation Conditions

Precultures of all microorganisms were cultivated in 250 mL shake flasks. The standard filling volumes were 10 mL, and all flasks were shaken at a frequency of $n = 350$ rpm and a shaking diameter of $d_0 = 50$ mm.

According to the literature (Ihling et al. 2018; Rahmen et al. 2015), two precultures were performed for *E. coli* BL21(DE3) pRotHi-YFP. The first preculture was conducted in terrific broth (TB) (Ihling et al. 2018) and inoculated with 100 µL from a cryoculture. The subsequent second preculture was inoculated to an initial OD_{600} of 0.1 from the first preculture. A non-inducing Wilms-MOPS mineral medium was used as a cultivation medium (Wilms et al. 2001). The non-inducing Wilms-MOPS medium contained 20 $g \cdot L^{-1}$ glucose as a single carbon source, 200 mM MOPS buffer and 0.5 $mg \cdot L^{-1}$ kanamycin (initial pH 7.5).

All monitored maincultures were inoculated with an initial OD_{600} of 0.1 from the second preculture. The cultivations were carried out in a modified Wilms-MOPS autoinduction medium. Instead of 5 $g \cdot L^{-1}$ Glycerol (Ihling et al. 2018; Rahmen et al. 2015), the modified Wilms-MOPS autoinduction medium contained only 4 $g \cdot L^{-1}$ glycerol, 2 $g \cdot L^{-1}$ lactose, and 0.5 $g \cdot L^{-1}$ glucose. Furthermore, 0.5 $mg \cdot L^{-1}$ kanamycin was added, and the initial pH was adjusted to 7.5 with 5 M NaOH. The filling volume in each of the 96 wells in the MTP (Riplate RW, 2.0 mL round deepwell plate, HJ-BIOANALYTIK GmbH, Erkelenz, Germany) was 0.5 mL, whereas the RAMOS shake flasks were filled with 10 mL of medium. Due to the medium's sufficient buffer capacity, the pH was not controlled. The cultivation temperature was set to 37°C. For cultivations in both, the µTOM (MTP) and RAMOS (shake flasks) devices, a shaking frequency of $n = 350$ rpm and a shaking diameter of $d_0 = 50$ mm were used.

The preculture of *H. polymorpha* RB11 pC10-FMD (P_{FMD}-GFP) was performed in Yeast Extract-Peptone-Glycerol (YPG) medium (Ausubel et al. 1989) containing 10 $g \cdot L^{-1}$ glycerol. The initial pH was set to 6.5 with 5 M NaOH, and the medium was inoculated with 100 µL from a cryoculture. The subsequent mainculture was inoculated with an initial OD_{600} of 0.05 in Yeast Extract-Peptone-Dextrose (YPD) medium containing 20 $g \cdot L^{-1}$ glucose (Ausubel et al. 1989). The initial pH was set to 6.5 with 5 M NaOH. In one MTP experiment, cultivations with filling volumes of 0.2, 0.4, and 0.5 mL were carried out in replicates of 24. The cultivation temperature was set to 37°C, a shaking frequency of $n = 350$ rpm and a shaking diameter of $d_0 = 50$ mm were used.

2.4 | Measurement Conditions in the µTOM and RAMOS Devices

The flow and stop phase duration for all cultivations conducted in the µTOM and RAMOS devices were set to 20 and 10 min, respectively (Anderlei and Büchs 2001; Anderlei et al. 2004; Schulte et al. 2018).

The flow of air into the measurement compartment of the µTOM was controlled to 2 volume air per volume of medium per minute (vvm). As the volume of the liquid medium, the total filling volume of the MTP was considered. A specific aeration rate of 2 vvm was set in reference to the total filling volume of the MTP. Thus, the total flow of air ($\dot{V}$) into the measurement compartment of the µTOM was set to 96 $SmL \cdot min^{-1}$ for an equal liquid filling volume of 0.5 mL in each well. For cultivations with an equal distribution of 0.2, 0.4, and 0.5 mL liquid filling volumes (24 wells each), the total filling volume of the MTP was 35.2 mL. Hence, the total flow of air was controlled to 70.4 $SmL \cdot min^{-1}$ to set a specific aeration rate of 2 vvm within the measurement compartment of the µTOM.

To ensure comparability between MTP and shake flask, the aeration rate in all cultivations conducted in the RAMOS device was set to 2 vvm for a fixed standard liquid filling volume of 10 mL.

All cultures were shaken and incubated in an incubation shaker (ISFX-1, Kuhner Shaker GmbH, Herzogenrath, Germany).

2.5 | Offline Analysis

2.5.1 | Optical Density

The initial optical density (OD_{600}) of each culture was measured using a spectrophotometer (GENESYS 20 Visible

Spectrophotometer, Thermo Scientific, Dreieich, Germany) at a fixed wavelength of 600 nm. All samples were measured in 1.5 mL microcuvettes (PS, Plastibrand, Roth, Karlsruhe, Germany). The samples were diluted with a 0.9% (w/v) NaCl solution, if the OD_{600} exceeded a value of 0.2.

2.5.2 | *pH Value*

The pH value of the unfiltered culture broth was measured at room temperature using a pH-meter (HI2211pH, Hanna Instruments, Vöhringen, Germany), equipped with a pH-electrode (InLab Easy pH, Mettler-Toledo, Giessen, Germany).

3 | Results and Discussion

3.1 | Description of the Sensor Setup in the μTOM Device

The μTOM device, used in this study, is based on the setup published by Dinger et al. (2022). A schematic representation of a cross-section of the μTOM device is depicted in Figure 1A. To allow monitoring of OTR and CTR, two types of sensors were implemented in the optoelectronic sensor module (Figure 1A, 1). The two sensors allow measuring the O_2 and CO_2 partial pressure (pO_2 and pCO_2) in separate wells of a 96-deepwell MTP (Figure 1A, 4). The current sensor layout of the optoelectronic sensor module is depicted in Figure 1B, and comprises 48 O_2- (Figure 1B, 13, green) and 48 CO_2-sensitive sensors (Figure 1B, 14, red). Both sensor types are bonded to the optoelectronic sensor module (Figure 1A, 1). In contrast to the O_2-sensitive sensors, an additional protection layer (Figure 1A, 15, dark blue), consisting of Hyflon AD 60, covers the CO_2-sensitive sensor. This amorphous perfluorinated polymer has been previously demonstrated to significantly delay poisoning of carbon dioxide sensors by volatile acidic species (Fritzsche et al. 2017).

To make the CO_2 "sensing chemistry" spectrally compatible with the optoelectronic components, a new indicator based on a diketopyrrolopyrrole dye class was synthesized (see Supporting Information 1–3). The new dye combines π-extended biphenyl substituents in diketopyrrolopyrrole (Schutting et al. 2013) with additional alkyl substituent at one of the nitrogen atoms, which enhances the photophysical properties, as described previously (Schutting et al. 2014). This compound can be conveniently prepared in only three steps from a cheap commercially available pigment. The new indicator shows pH-dependent excitation and emission spectra (see Supporting Information 4). Although both forms, in principle, can be utilized for CO_2 sensing, this work made use of the deprotonated form of the dye, that is spectrally compatible to the excitation wavelength (~625 nm) and the far-red emission detection window. Thus, in the current read-out scheme, the indicator shows high fluorescence intensity in the absence of CO_2 (due to the presence of a lipophilic base in the sensing membrane) and low fluorescence upon protonation in presence of CO_2 (Supporting Information 4 and 5). Finally, in order to utilize a DLR referencing scheme, Egyptian blue microcrystalline powder as an inert reference emitter was added (Borisov et al. 2013). As can be seen, the pigment also is efficiently excitable with the red light and shows emission above 700 nm (Supporting Information 4).

The MTP within the housing of the μTOM device (Figure 1A, 3) is placed on a mounting tray (Figure 1A, 5). A vertical lifting

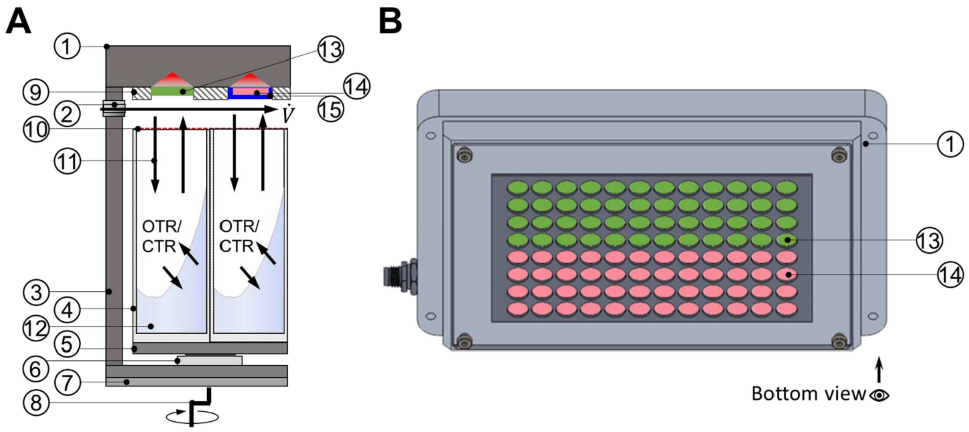

FIGURE 1 | Schematic representation of the μTOM device with integrated O_2 and CO_2 sensors. (A) Cross-section of two measurement positions (wells) within the μTOM device. The optoelectronic sensor module (1) allows for measuring the O_2 and CO_2 partial pressure (pO_2 and pCO_2) separately within the wells of a 96-deepwell microtiter plate (MTP) (4). To ensure sterile cultivation conditions, the MTP is covered with an adhesive sterile sealing film (10). The MTP within the housing of the μTOM device (3) is placed on a mounting tray (5). A lifting mechanism (6) can vertically lift the mounting tray, to close the headspace of every well. The housing is fixed to a shaker tray (7). The shaker tray is mounted on an orbital shaker (8) within a temperature-controlled incubation hood. Humidified filtered air with a specific air flow ($\dot{V}$) enters the housing through four ventilation ports (2) and, hence, ventilates the wells of the MTP (11). The respiration activity of microbial cultures (12) within the wells leads to specific oxygen (OTR) and carbon dioxide transfer rates (CTR) within each well. The OTR and CTR can be measured by assessing the pO_2 and pCO_2 over time during a so-called stop phase (Supporting Information 6), described in the literature (Dinger et al. 2022). During the stop phase, the MTP is lifted and pressed against the sealing layer (9) to gas-tightly seal each well. The pO_2 and pCO_2 are measured via O_2 (13) and CO_2-sensitive sensors (14). Both sensor types are bonded to the optoelectronic sensor module (1). An additional protection layer (15), consisting of Hyflon AD60, covers the CO_2-sensitive sensor. (B) Bottom view of the optoelectronic sensor module (1). The sensor layout is composed of 48 O_2 (13, green) and 48 CO_2 (14, red) sensors (sensors not accurate to size).

mechanism (Figure 1A, 6) of the mounting tray allows to close the headspace of every well. The housing is fixed to a shaker tray (Figure 1A, 7). The shaker tray is mounted on an orbital shaker (Figure 1A, 8) within an incubation hood. During a flow phase, humidified filtered air with a specific air flow ($\dot{V}$) enters the housing through ventilation ports (Figure 1A, 2). The respiration activity of microbial cultures (Figure 1A, 12) leads to specific oxygen (OTR) and carbon dioxide transfer rates (CTR) within each well. The OTR and CTR can be measured by assessing the pO_2 and pCO_2 partial pressure over time during a so-called stop phase. During the stop phase, the MTP is lifted and pressed against the sealing layer (Figure 1A, 9) to seal each well gas-tightly. The flow and stop phase are schematically shown in Supporting Information 6 and were previously described by Dinger et al. (2022). Flow and stop phase are periodically repeated throughout a cultivation in the μTOM device.

An exemplary course of the pCO_2 during a cultivation of the yeast *Hansenula polymorpha* is shown in Figure 2. In the case of an aerobic cultivation, the metabolic activity leads to CO_2 evolution from the culture broth. During the stop phase this results in a linear increase in the pCO_2 and vice versa the oxygen partial pressure decreases, due the respiration activity.

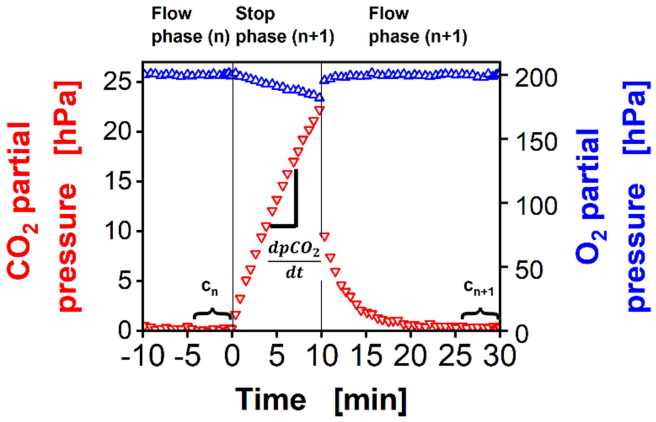

FIGURE 2 | Typical course of the carbon dioxide partial pressure (pCO_2, red downward triangles) and the oxygen partial pressure (pO_2, blue upward triangles) during one measurement cycle ($n+1$), consisting of a flow (20 min) and a stop phase (10 min). Cycle $n+1$ follows a previous cycle n. The cycles periodically continue throughout the whole cultivation. A schematic representation of the μTOM device during flow and stop phase is presented in Supporting Information 6. The pO_2 and pCO_2 above 96 (48 CO_2 and 48 O_2 sensors) separate replicate MTP wells are individually measured continuously throughout the whole cultivation. During the stop phase, the carbon dioxide partial pressure increases linearly and vice versa the oxygen partial pressure decreases, due to the respiration activity of the cultivated microorganisms. The linear slopes of the changing partial pressures are used to calculate the carbon dioxide and oxygen transfer rates (CTR and OTR). The slope of the carbon dioxide partial pressure $\frac{dpCO_2}{dt}$ is depicted and the CTR is calculated from the slope according to Equation 1. For the online calibration of the CO_2-sensitive sensors, an arithmetic mean value of the pCO_2 of 20 measurement points (roughly 2.5 min) at the end of each flow phase, representing the phase shift in air ($d\varphi_{air}$), is calculated. Calibrations in cycle n and cycle $n+1$ are marked as C_n and C_{n+1}, respectively.

From the measured change of the pCO_2 over time during the stop phase, the CTR can be calculated according to Equation 1 (Anderlei et al. 2004):

$$\mathrm{CTR} = \frac{dp_{CO_2}}{dt}\frac{V_G}{V_L \cdot R \cdot T} \quad (1)$$

where CTR [$mmol \cdot L^{-1} \cdot h^{-1}$] is the carbon dioxide transfer rate, $\frac{dp_{CO2}}{dt}$ [$Pa \cdot h^{-1}$] is the change of the carbon dioxide partial pressure over time, V_G [L] is the gas volume of the headspace in the sealed well during the stop phase, R [$L \cdot Pa \cdot mol^{-1} \cdot K^{-1}$] is the universal gas constant, T [K] is the cultivation temperature, and V_L [L] is the liquid filling volume of the well. The changes in the partial pressures are an inherent effect of the stop phase, where the wells are gas-tightly sealed. However, even at high respiration activities of about 60 mmol/L/h the oxygen partial pressure only decreases by roughly 30 hPa (from ~200 hPa for air to ~170 hPa) and is not depleted. Therefore, the stop phase does not affect the culture by oxygen limitation, and hence, does not impact OTR and CTR measurement. In fact, the length of the stop phase can be used to adjust the measurement sensitivity of the μTOM (Dinger et al. 2022) according to the requirement of the investigated biological system, in the same way as for the RAMOS technology in shake flasks (Anderlei and Büchs 2001; Anderlei et al. 2004). For cultures with low respiration activities like cell cultures stop phase durations up to 20 min can be applied to increase the change in partial pressures (Ihling et al. 2021; Neuss et al. 2025). On the other hand, for high respiration activities a stop phase length of 5 min is sufficient (Forsten et al. 2024). A mathematical description for choosing the optimal length of the stop phase for expected OTRs of the cultures was published by Dinger et al. (2022). Extreme cases for aerobic cultivations are oxygen limited cultivation conditions, where the OTR of the cultures exceeds the maximum oxygen transfer capacity between gas and liquid phase. If not desired, these conditions lead to metabolic changes, compared to aerobic conditions. However, oxygen limited conditions can be prevented by increasing the shaking frequency or reducing the liquid filling volume. Both factors have been studied in detail and were empirically correlated to the OTR_{max} in the μTOM by Dinger et al. (2022).

3.2 | Characterization of CO_2-Sensor Response and Drift

To measure the pCO_2 correctly, the CO_2-sensors must be calibrated before any experiment. Additionally, for the CO_2-sensors an online recalibration during cultivations must be performed to correct for the sensor drift. The calibration procedures are described in this section. To characterize the response of the sensors to changes in pCO_2, a calibration setup (Supporting Information 7) was used, which is schematically shown in Figure 3. The setup allows to control a specific pCO_2 within a calibration cell (Figure 3F), housing the CO_2-sensors. Four Pico-O_2 modules (PyroScience, Aachen, Germany) (Figure 3, 1–4) measure the sensor responses. A Pico-O_2 module is an optoelectronic measuring module with equivalent functionality compared to one measuring position of the μTOM optoelectronic sensor module (Figure 1A, 1). The pCO_2 within the

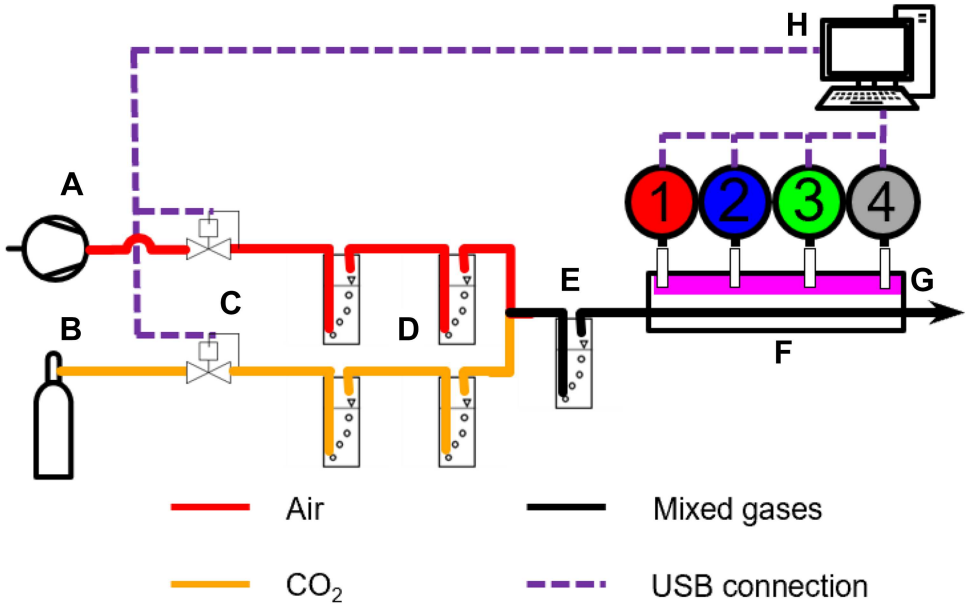

FIGURE 3 | Schematic representation of the calibration setup. The calibration setup is supplied with air by a compressor (a), and pure CO_2, which is taken from a gas cylinder (b). Two mass flow controllers (c) control the air and CO_2 flow through gas washing bottles (d) and the calibration cell (f), housing the CO_2 sensors. The mixing of specific air (red line) and CO_2 (orange line) flows allows to adjust the CO_2 partial pressure (pCO_2) within the calibration cell (f). Only the lower surface of the CO_2 sensors (magenta line, g) is in contact with the gas phase below the sensors within the calibration cell. The PC (h) is used to set the flows of the two mass flow controllers via a USB connection (dashed purple line). The absolute flow through the cell (f) is kept constant at 200 $SmL \cdot min^{-1}$. An additional gas washing bottle (e) can optionally be added, to mix both gas flows (black line). Furthermore, the additional gas washing bottle contained 1 $g \cdot L^{-1}$ acetic acid, to test the sensor's sensitivity toward acidic compounds. The response of the CO_2 sensors (magenta line, g) inside the calibration cell (f) is monitored by four optoelectronic devices, so-called Pico-O_2 modules (1, 2, 3, 4). These were connected to the PC (h) via a USB connection (dashed purple line).

calibration cell is changed by a mixed flow of compressed air (Figure 3A) and pure CO_2 (Figure 3B). The flows of both gases are controlled by two mass flow controllers (Figure 3C) and are humidified in two gas washing bottles each (Figure 3D), before entering the calibration cell. While the absolute flow through the calibration cell is kept constant at 200 $SmL \cdot min^{-1}$, the ratio between compressed air and pure CO_2 is changed to adjust a specific pCO_2 within the calibration cell. The calibration setup operates fully automatically, and an external computer (Figure 3H) records the sensor responses. A calibration routine within the calibration setup is periodically repeated (see Figure 4). Each calibration procedure lasts 28 min and includes seven pCO_2 setpoints ranging from 0.39 to ~47 hPa. First, the seven setpoints are reached by increasing the pCO_2 and subsequently by decreasing the pCO_2. During 15 min, the pCO_2 increased stepwise (every 2 min). Subsequently, the pCO_2 is decreased stepwise in the opposite direction. By both, increasing and decreasing the pCO_2, not only were the sensors calibrated, but also the ability of the sensors to recover from exposure to CO_2 was proven. The response time to reach 90% of the sensor signal at the setpoints shown in Figure 4 is roughly 15 s. Therefore, the sensor response does not delay the measured CO_2 partial pressure during a 10 min long stop phase as depicted in Figure 2.

The sensing principle of the CO_2-sensors relies on the protonation of the indicator in presence of CO_2 (Supporting Information 5). The resulting hypsochromic shift of absorption and emission bands can be measured as an increase of the phase shift ($d\varphi$) by the optoelectronics of the μTOM device. The arithmetic means and standard deviations of five measurement points of four sensors at each adjusted pCO_2 are shown in Figure 4B. By optimizing the parameters a_0, $b_{0,0}$ and $b_{1,0}$ using the downhill simplex method, the calibration curve (Equation 2) was fitted to the calibration points. The results of the calibration procedure and the fitted calibration curve are shown in Figure 4B.

$$pCO_2 = \frac{\left((b_{0,0} + (a_{0,0} \cdot b_{1,0}))\frac{d\varphi}{d\varphi_{air}}\right) - a_{0,0}}{1 - b_{1,0} \cdot \frac{d\varphi}{d\varphi_{air}}} \quad (2)$$

where pCO_2 is the carbon dioxide partial pressure, a_0, $b_{0,0}$ and $b_{1,0}$ are fit parameters of the calibration equation and $\frac{d\varphi}{d\varphi_{air}}$ is the measured phase shift relative to the phase shift in air. The pCO_2 is calculated from the sensor response (phase shift, $d\varphi$) in the form of the relative phase shift. The relative phase shift is calculated by dividing the measured $d\varphi$ by the initially measured phase shift in air ($d\varphi_{air}$).

The calibration procedure, shown in Figure 4A, was repeated twice per hour for 96 h. To investigate the sensor drift, the measured phase shift in air ($d\varphi_{air}$) at the beginning of each calibration routine is divided by the phase shift in air ($d\varphi_{air,0}$) of the first calibration. In this way, the relative sensor drift is calculated $\left(\frac{d\varphi_{air}}{d\varphi_{air,0}}\right)$. The progression of the relative phase shifts follows a linearly increasing trend (Figure 5A, black triangles), showing a continuous drift. Although the exact origin of the

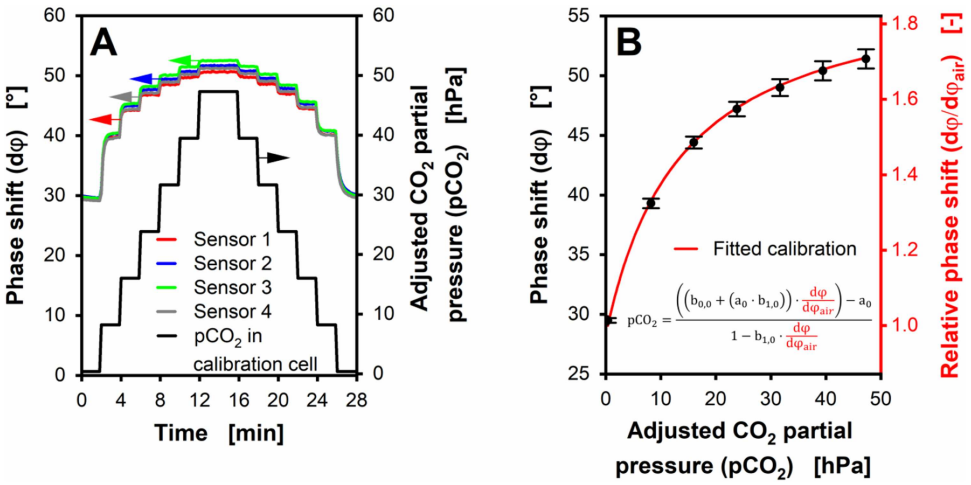

FIGURE 4 | (A) Typical results of the calibration procedure, conducted with the calibration setup illustrated in Figure 3. A picture of the setup is shown in Supporting Information 7. In a period of 16 min of calibration, the CO_2 partial pressure (pCO_2) within the calibration cell was gradually increased every 2 min from 0.39 to 47.29 hPa. After 16 min of calibration, a stepwise decrease of the pCO_2 back to 0.39 hPa followed. The sensor responses to pCO_2 changes within the calibration cell were continuously measured using the four Pico-O_2 devices presented in Figure 3. The sensor response is measured as the phase shift between the sinusoidal intensity-modulated excitation light and the resulting fluorescence signal of the CO_2 sensor. (B) Determination of initial calibration parameters from the calibration procedure in (A). The mean average of the relative phase shift of four CO_2 sensors at seven calibration points with pCO_2 ranging from 0.39 hPa to 47.29 hPa is depicted as black dots. The error bars represent the mean standard deviation. The calibration model (Equation 2) was fitted to the relative phase shift values $\frac{d\varphi}{d\varphi_{air}}$. The relative phase shift represents the phase shift at an adjusted pCO_2, normalized with the phase shift in air (0.39 hPa CO_2). The calibration was performed at a temperature of 37°C.

drift could not be clarified, the phenomenon is likely to originate from an irreversible reaction of traces of acidic species with the lipophilic base. This results in decrease fluorescence from the deprotonated form of the dye and, thus, in an increase of the measured phase shift, which reflects the increasing contribution of the reference phosphor material. In fact, spiking the fifth gas washing bottle (Figure 3E) with 1 g·L^{-1} acetic acid resulted in an airflow containing traces of acetic acid, which accelerated the relative sensor drift (Figure 5A, colored squares), compared with exposure to ambient air (Figure 5A, black triangles). In conclusion, it can be assessed that although Hyflon AD60 layer was previously demonstrated to significantly enhance the long-term stability of the CO_2 sensors, acidic compounds still permeate this layer of the CO_2 sensors. It is also possible that this protective layer is less efficient after integration of the sensor films due to structural defects, such as partial delamination of the Hyflon AD60 layer. Throughout the first 70 h of exposure (Figure 5A) to air containing traces of acetic acid, the calibration procedure shown in Figure 4A is performed 2 times per hour. The starting point of each calibration in air containing traces of acetic acid is shown in Figure 5A (colored squares). The relative phase shifts during each calibration procedure are presented in Figure 5B. The time point of each calibration procedure is marked by the scale legend in Figure 5B. The sensor drift leads to a decrease in the measured relative phase shift over time at the different calibration points. After 70 h of exposure to an airflow containing traces of acetic acid, the measured relative phase shift at the highest calibration point with a pCO_2 of 47.29 hPa decreased from 1.6 to 1.3 (Figure 5B). Hence, the dynamic range of the CO_2 sensors is reduced by two-fold. A two-fold reduced dynamic range also leads to a two-fold decreased signal-to-noise ratio. In Figure 5A, the time point of the two-fold reduced dynamic range after 70 h is marked by a vertical red dashed line. At this point, a relative sensor drift with a value of 1.5 can be measured (Figure 5A, horizontal red dashed line). Without a continuous recalibration of the CO_2 sensors, the sensor drift results in an overestimation of the measured pCO_2, preventing accurate CTR calculations. However, a continuous recalibration of the CO_2-sensor at seven adjusted pCO_2 during cultivations in the μTOM device is not feasible. The removal of the sensors for calibration or an in situ calibration at increased pCO_2 in the μTOM would directly affect the cultivation conditions.

To overcome this challenge, a method to recalibrate the CO_2 sensors online based on the relative sensor drift was developed. A flow chart of the full sensor drift compensation and online recalibration is presented in Supporting Information 8. For each produced sensor batch, four sensors are sacrificed to calculate the initial calibration parameters ($a_{0,0}$, $b_{0,0}$, $b_{1,0}$) of Equation 2 by performing the calibration procedure depicted in Figure 4. Subsequently, the sensor drift is characterized by spiking the fifth gas washing bottle (Figure 3E) with 1 g·L^{-1} acetic acid. As shown in Figure 5B, throughout the exposure of the sensors to an airflow containing traces of acetic acid, the calibration procedure is repeated twice per hour. In Figure 5C,D it is shown that the refitted calibration parameters $b_{0,d}$ and $b_{1,d}$, normalized to the initially calculated parameter $b_{0,0}$, and $b_{1,0}$ $\left(\frac{b_{0,d}}{b_{0,0}} \text{ and } \frac{b_{1,d}}{b_{1,0}}, \text{respectively}\right)$ of four CO_2 sensors, show a linear dependence of the relative sensor drift (Figure 5C,D, black dashed lines). A similar linear dependency was observed for the parameter $a_{o,d}$, which is depicted in Supporting Information 9.

During cultivation in the μTOM, both calibration parameters $b_{0,d}$ and $b_{1,d}$ can be estimated as a function of the relative sensor drift and their initial values $b_{0,0}$, and $b_{1,0}$. Finally, the third calibration parameter $a_{0,d}$ is optimized using the downhill

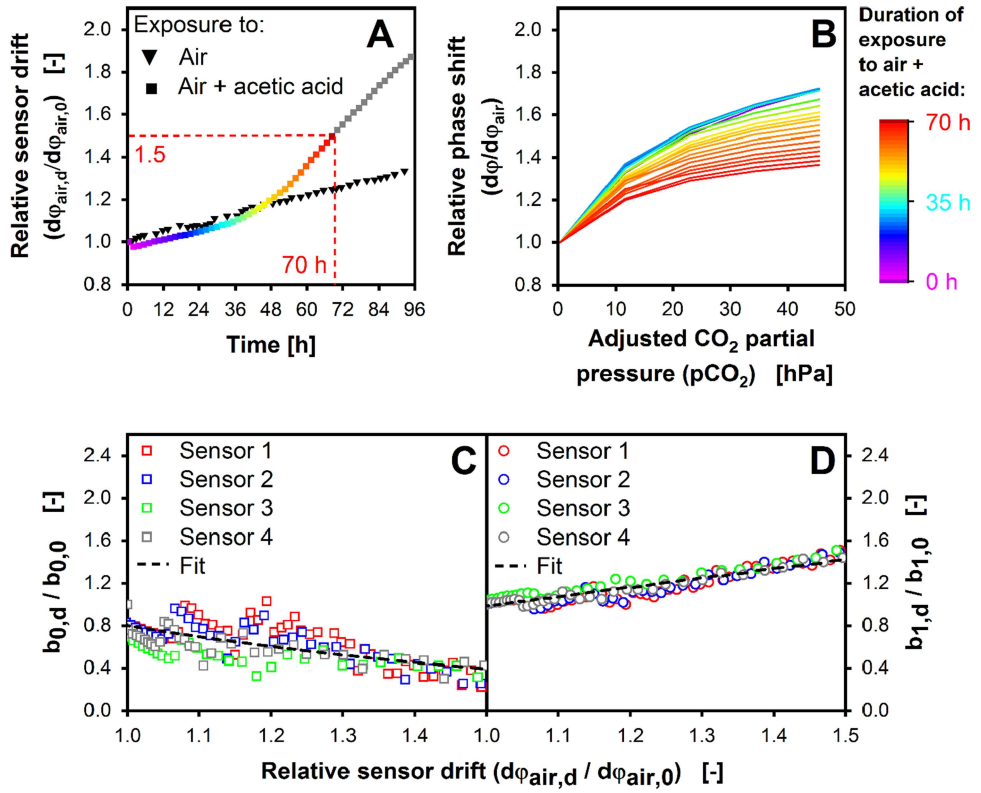

FIGURE 5 | Characterization of the drift behavior of the CO_2 sensors. (A) The exemplary drift of the continuously measured relative phase shift over 96 h. One CO_2 sensor was exposed to humidified air (—▼—), and the second sensor was exposed to air humidified with water containing 1 g·L^{-1} acetic acid (—■—). (B) Relative phase shift at adjusted CO_2 partial pressures (0.39–47.29 hPa) of the CO_2 sensor humidified with water containing 1 g·L^{-1} acetic acid during 70 h of continuous exposure (A). The scale legend in (B) shows the time period when the calibration routine was performed. The starting points of each calibration procedure in (B) are marked in the same color in (A). Calibration procedures with a relative phase shift in air larger than 1.5 (reached after 70 h) of exposure were not considered for the characterization of the drift behavior of the sensors. The calibration procedure, shown in Figure 4A, was periodically repeated (2 times per hour) during the 70 h of exposure. After each calibration procedure, the parameters of the calibration model (Equation 2) were refitted to the relative phase shifts shown in B. The refitted calibration parameters $b_{0,d}$ and $b_{1,d}$ normalized to the initial parameter $b_{0,0}$ and $b_{1,0}$ $\left(\frac{b_{0,d}}{b_{0,0}} \text{ and } \frac{b_{1,d}}{b_{1,0}}, \text{respectively}\right)$ of four CO_2 sensors are shown in C and D as a function of the current phase shift in air ($d\phi_{\text{air}}$), normalized with the phase shift in air at 0 h of exposure to acetic acid ($d\phi_{\text{air},0}$). A linear fit for all normalized calibration parameters $\frac{b_{0,d}}{b_{0,0}}$ and $\frac{b_{1,d}}{b_{1,0}}$ was calculated and is depicted as a black dashed line in C and D. The values for $a_{0,d}$ are shown in the Supporting Information 9.

simplex method, to fit the calibration curve to the one-point calibration point in air at the end of each stop phase (Figure 2, C_n). By using the drift-compensated calibration parameters $a_{0,d}$, $b_{0,d}$, and $b_{1,d}$ in Equation 3, the pCO_2 can be measured accurately in the μTOM device.

$$pCO_2 = \frac{\left((b_{0,d} + (a_{0,d} \cdot b_{1,d}))\frac{d\varphi}{d\varphi_{\text{air}}}\right) - a_{0,d}}{1 - b_{1,d} \cdot \frac{d\varphi}{d\varphi_{\text{air}}}} \quad (3)$$

By applying this method, cultivations of yeast and bacteria were monitored online. The results are shown in the following sections.

3.3 | Cultivation of *Hansenula polymorpha* (*Ogataea angusta*)

Parallel cultivations of *Hansenula polymorpha* RB11 pC10-*FMD* (P_{FMD}-GFP) (henceforth referred to as *H. polymorpha)* on YPD medium supplemented with 20 g/L glucose were conducted in the μTOM device measuring OTR and CTR. Cultivations with three different filling volumes were monitored, and the influence of oxygen limitation on the cultivation results was analyzed.

Cultivations with filling volumes of 0.2 and 0.4–0.5 mL were performed in 24 replicates each (two rows of the MTP for each filling volume). For each filling volume, the OTR and CTR were measured separately in 12 of the 24 replicate cultivations. The RQ is calculated from simultaneous measurement of CTR and OTR in separate replicate wells. The sensor layout and the well pairing are depicted in Supporting Information 13. The results of the cultivations are depicted in Figure 6. Each cultivation showed an equivalent exponential increase of the OTR and the CTR, resulting in an RQ value close to 1, as shown in Figure 6D–F. The maximum OTR reached during the cultivations of *H. polymorpha* decreased with increasing filling volumes. The end of the oxygen-unlimited growth phases for each cultivation condition is marked by vertical light blue dashed lines in Figure 6. The maximum measured OTR is limited by

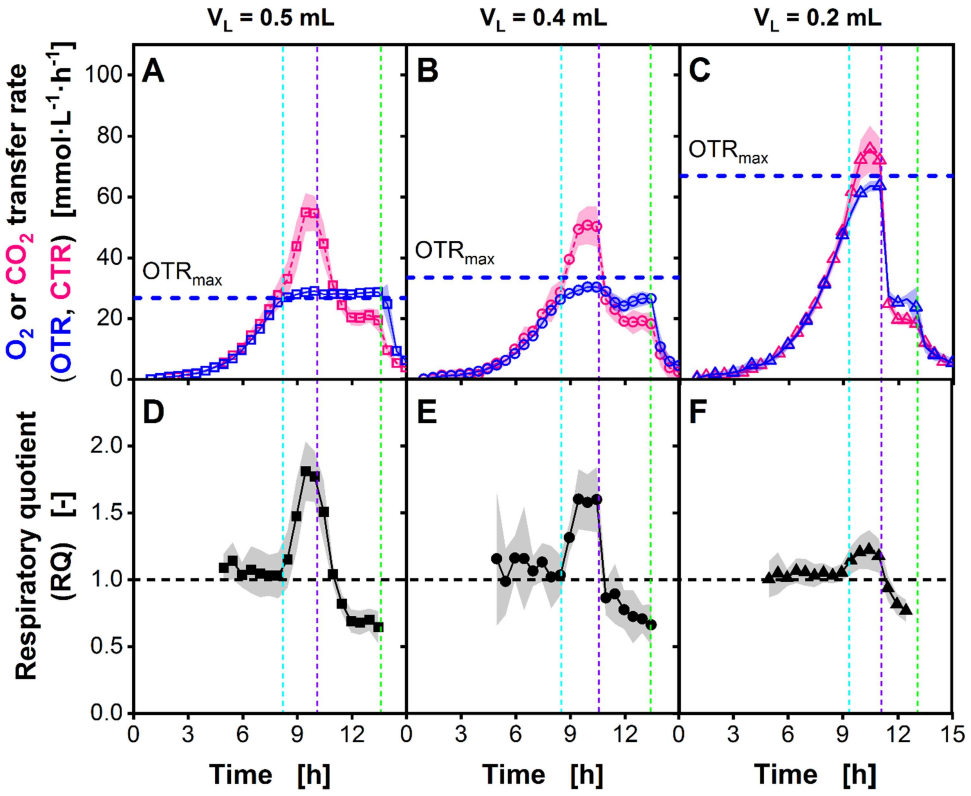

FIGURE 6 | Course of oxygen (OTR, blue) and carbon dioxide transfer rates (CTR, magenta) and the respiratory quotient (RQ, black) in parallel cultivations of *Hansenula polymorpha* RB11 pC10-*FMD* (PFMD-GFP). The average values and mean standard deviations of 12 replicates are depicted as symbols and shadows, respectively. The parallel cultivations were performed with three filling volumes, 0.5 mL (—□—, A, D), 0.4 mL (—○—, B, E), and 0.2 mL (—△—, C, F), resulting in specific maximum oxygen transfer capacities (OTR_{max}, horizontal blue dashed line), as published by Dinger et al. (2022). A respiration quotient of 1 is indicated by a horizontal black dashed line (D, E, F). OTR values below 4 $mmol \cdot L^{-1} \cdot h^{-1}$ were not considered for the calculation of the RQ. The light blue vertical dashed lines mark the end of the oxygen-unlimited growth phase, purple vertical dashed lines indicate the depletion of glucose, and light green vertical dashed lines indicate the depletion of all carbon sources in the medium. Cultivation medium: complex YPD medium, carbon source: 20 $g \cdot L^{-1}$ glucose. Cultivation conditions: 96-deepwell MTP (round), shaking frequency $n = 350$ rpm, shaking diameter $d_0 = 50$ mm, $T = 37°C$, aeration: 2 vvm, flow phase: 20 min, stop phase: 10 min.

the maximum oxygen transfer capacity (OTR_{max}) in the wells, resulting from the filling volume and the shaking conditions. The theoretical OTR_{max} was calculated according to Dinger et al. (2022) (Supporting Information 10) for each filling volume is depicted in Figure 6A–C as a thick horizontal dashed blue line. The calculated OTR_{max} values are 67.0, 33.5, and 26.8 $mmol \cdot L^{-1} \cdot h^{-1}$ for a filling volume 0.2, 0.4, and 0.5 mL, respectively, at a shaking frequency of 350 rpm and shaking diameter of 50 mm. The measured values for each filling volume are within a 10 percent range of the calculated OTR_{max} values and, therefore, in good agreement with the correlation published by Dinger et al. (2022). In contrast to the OTR, the CTR cannot be limited, since the evolved CO_2 is transferred out of the liquid medium. Therefore, an increase of the CTR, exceeding the OTR, was measured in each cultivation. As a result, the RQ value reaches values significantly higher than 1 (Figure 6D–F). The increased RQ results from the partially anaerobic metabolism of *H. polymorpha* under oxygen-limited cultivation conditions with glucose as substrate. The partially anaerobic metabolism (Pasteur effect) results in the formation of ethanol and acetic acid as products and, hence, in an increase in the RQ (Stockmann et al. 2003; Stöckmann et al. 2003). For each cultivation, a gradual decrease in the CTR is visible after 9–10 h of cultivation, marking the time point of glucose depletion (vertical purple dashed lines in Figure 6). After glucose depletion, the previously oxygen-limited cultures show a decrease in CTR, indicating the consumption of ethanol and acetic acid. The measured RQ decreases to a value below 1, when ethanol is consumed. This is due to its higher degree of reduction (Supporting Information 11), compared with glucose (6 and 4, respectively). The resulting RQ values below 1 have already been published for *H. polymorpha* (Stockmann et al. 2003) and other yeasts like *Pichia stipites* or *Saccharomyces cerevisiae* (Anderlei et al. 2004). Based on the final gradual decrease of the OTR and CTR, the depletion of all carbon sources in the liquid media can be concluded (Figure 6A–C, vertical light green dashed lines).

The combined measurement of the OTR and CTR allows characterizing the metabolism of aerobic cultivations in liquid volumes below 1 mL. Furthermore, phases of oxygen-unlimited and partially anaerobic metabolism can be distinguished. Furthermore, the consumption of the ethanol, which was prior produced due to oxygen limitation could be detected. In case of the cultivation conditions depicted in Figure 6A,D, the switch between ethanol production and consumption would remain undiscovered, if only the OTR would be measured. Thus, combined measurement of OTR and CTR allows a better understanding of bioprocesses.

3.4 | Cultivation of *Escherichia coli*

One frequently applied method for classifying the performance of recombinant clone libraries of *Escherichia coli* producing heterologous enzymes is the cultivation on Wilms-MOPS auto-induction medium (Rahmen et al. 2015). The Wilms-MOPS auto-induction medium used in this experiment contains glucose, lactose and glycerol as carbon sources that are sequentially or co-consumed by the organisms. The depletion of the individual carbon sources was detected by HPLC analysis and first published by medium (Rahmen et al. 2015). However, due to the different degrees of reduction (Supporting Information 12) of glucose, lactose, and glycerol (4, 4, and 4.67, respectively) the sequential consumption of the three carbon sources is detectable by the measured RQ.

Figure 7 shows the measured averaged OTR, CTR, and RQ values from 96 wells (Figure 7A,C) and six shake flasks (Figure 7B,D). The pairing of the wells for simultaneous OTR, CTR, and RQ measurements in separate replicate wells is depicted in Supporting Information 13. The pooled standard deviation of the CTR measurements in the µTOM was 1.4 mmol·L^{-1}·h^{-1}. As a quantitative cutoff for RQ calculation a limit of detection (threefold pooled standard deviation ~4 mmol·L^{-1}·h^{-1}) was defined for the CTR measurement. The limit of detection can be improved by optimizing the length of the stop phase as mathematically described by Dinger et al. (2022). The cutoff value for the CTR does not impact the independent subsequent CTR measurements technically or mathematically. The results in this study are well comparable to the extensive studies on the Wilms-MOPS auto-induction medium described by Rahmen et al. (2015) and Ihling et al. (2018). The cultivation pattern of *E. coli* BL21(DE3) pRotHi-YFP in Wilms-MOPS auto-induction medium can be divided into four characteristic phases. The end of phases I, II, and III are characterized by the depletion of either glucose, lactose, or glycerol, respectively. A detailed description of the phases observed for the cultivation of *E. coli* in auto-induction medium has previously been published (Ihling et al. 2018; Rahmen et al. 2015; Rahmen et al. 2015). Additionally, cultivation results and HPLC-analyses for the particular strain, used in this study, were reported in the literature (Flitsch et al. 2016). The yield coefficients for biomass growth on glucose and glycerol (0.5 and 0.44, respectively) were taken from the results published by Kopp et al. (2017). Contrary to the higher degree of reduction of glycerol compared with glucose, the biomass yield of the plasmid-containing *E. coli* BL21 (DE3) strains on glycerol is lower than the biomass yield on glucose. However, for strains without plasmids, biomass yields of 0.55 with glycerol as substrate were reported (Kopp et al. 2017). For the elemental composition of the biomass, the empirical formula $CH_2N_{0.25}O_{0.5}$ was used (Atkinson and Mavituna 1982). The resulting estimated stoichiometry for the growth on glucose and glycerol is presented in Equations 4 and 7, respectively. The stoichiometric amount of biomass ($\nu_{Biomass}$) for growth on glucose and glycerol

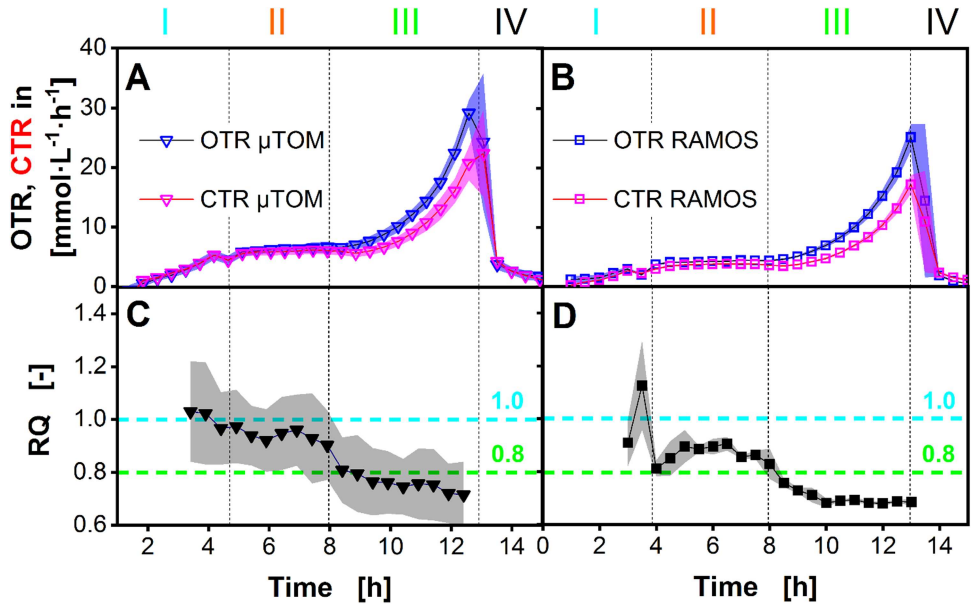

FIGURE 7 | Comparison of the oxygen (OTR, blue) and carbon dioxide transfer rates (CTR, magenta) and the respiration quotient (RQ, black) in parallel cultivations of *E. coli* BL21(DE3) pRotHi-YFP. (A and C) The cultivations were carried out in each well of a 96-deepwell microtiter plate (MTP) of the novel µTOM device (—∇—) and (B and D) in eight shake flasks in a RAMOS device (—□—). The average values and mean standard deviations of the parallel cultivations are depicted as symbols and shadows, respectively. In the µTOM device OTR and CTR values were each calculated from 48 replicate cultivations. In the RAMOS device 4 replicate cultivations were evaluated. The Roman numbers represent the different cultivation phases, according to Rahmen et al. (2015), separated by dashed vertical lines. (I): Pure glucose consumption (resulting in RQ ≥ 1, light blue horizontal dashed line), (II) induction phase with parallel consumption of glycerol and lactose, (III) growth on glycerol (resulting in RQ ≤ 0.8, green horizontal dashed line), and (IV) end of active respiration, due to carbon source depletion. CTR values below 4 mmol·L^{-1}·h^{-1} were not considered for the calculation of the RQ. Cultivation medium: Mineral Wilms-MOPS autoinduction medium, carbon sources: 0.5 g·L^{-1} glucose, 2 g·L^{-1} lactose, and 4 g·L^{-1} glycerol. Cultivation conditions µTOM: 96-round deepwell MTP, filling volume $V_L = 0.5$ mL, shaking frequency $n =$ 350 rpm, shaking diameter $d_0 = 50$ mm, $T = 37$°C, aeration = 2 vvm, flow phase: 20 min, stop phase: 10 min, 48 replicate. RAMOS: 250 mL shake flasks, $V_L = 10$ mL, $n = 350$ rpm, $d_0 = 50$ mm, $T = 37$°C, aeration: 2 vvm, flow phase: 20 min, stop phase: 10 min.

is calculated according to Equations 3 and 6, respectively. Where $M_{Glucose}$ is the molar mass of glucose, $M_{Biomass}$ is the molar mass of the biomass ($CH_2N_{0.25}O_{0.5}$), $M_{Glycerol}$ is the molar mass of glycerol, $Y_{\frac{Biomass}{Glucose}}$ is the biomass yield for growth on glucose, and $Y_{\frac{Biomass}{Glycerol}}$ is the biomass yield for growth on glycerol. The theoretical RQ values, resulting from the reaction stoichiometry for growth on glucose and glycerol, are 1.17 (Equation 5) and 0.74 (Equation 8), respectively.

Stoichiometry for growth on glucose (Biomass Yield: 0.5):

$$\nu_{Biomass} = Y_{\frac{Biomass}{Glucose}} \cdot \frac{M_{Glucose}}{M_{Biomass}} = 0.5 \cdot \frac{180 \frac{g}{mol}}{21.51 \frac{g}{mol}} = 4.18 \quad (3)$$

$$C_6H_{12}O_6 + 1.05\ NH_3 + 1.55\ O_2 \rightarrow 4.18\ CH_2N_{0.25}O_{0.5} + 1.82\ CO_2 + 3.38\ H_2O \quad (4)$$

$$RQ = \frac{n_{CO_2}}{n_{O_2}} = \frac{1.82\ mol}{1.55\ mol} = 1.17\ [-] \quad (5)$$

Stoichiometry for growth on glycerol (Biomass Yield: 0.44):

$$\nu_{Biomass} = Y_{\frac{Biomass}{Glycerol}} \cdot \frac{M_{Glycerol}}{M_{Biomass}} = 0.44 \cdot \frac{92.1 \frac{g}{mol}}{21.51 \frac{g}{mol}} = 1.88 \quad (6)$$

$$C_3H_8O_3 + 0.47\ NH_3 + 1.50\ O_2 \rightarrow 1.88\ CH_2N_{0.25}O_{0.5} + 1.12\ CO_2 + 2.82\ H_2O \quad (7)$$

$$RQ = \frac{n_{CO_2}}{n_{O_2}} = \frac{1.12\ mol}{1.50\ mol} = 0.74\ [-] \quad (8)$$

The results in Figure 7C,D show that the measured RQ value during phase I is larger 1 (light blue horizontal dashed lines), indicating growth on glucose, as estimated by Equations 3 and 4. The end of phase I and, hence, the depletion of glucose is marked by a typically short decrease of the OTR and CTR values (around 5 $mmol \cdot L^{-1} \cdot h^{-1}$) after around 5 h of cultivation. Throughout phase 3, the OTR and CTR are exponentially increasing, indicating growth of the microorganisms. The measured RQ values are within the range of the theoretical RQ of 0.74 (green horizontal dashed line), thus, indicating the consumption solely of glycerol. The consumption of glycerol results in exponential growth and consequently in an exponential increase of OTR and CTR, until glycerol is depleted after about 13 h of cultivation (see Figure 7A,B). In phase II, the RQ value is in a range between 1.17 (Equation 5) and 0.74 (Equation 8), indicating neither growth solely on glucose nor glycerol. Flitsch et al. (2016) and Rahmen et al. (2015) could show that during phase II the organisms consume lactose and glycerol in parallel. The consumption of lactose leads to an induction of the protein production. The resulting metabolic burden (Ihling et al. 2018; Rahmen et al. 2015) leads to constant OTR and CTR levels between 5 and 8 h of cultivation (see Figure 7A,B, phase II).

By comparing the RQ progression during cultivations of *E. coli* with the theoretical stoichiometry of the metabolic activity of the microorganisms, the consumed carbon source can be identified online. Additionally, the results in Figure 7 indicate an insufficient ratio between lactose and glycerol in the medium. The ratio leads to a second undesired growth phase (phase III) on glycerol. In an efficient bioprocess, this second growth phase (Figure 7, phase III) must be minimized by optimizing the ratios of the three carbon sources, as shown by Kunze et al. (2012). The optimization can be performed in subsequent high-throughput screening experiments (24 quadruplicate cultivations) in 96-deepwell MTPs, cultivated in the novel µTOM device. Furthermore, parallel experiments in the µTOM and the RAMOS demonstrated good agreement between both systems. The arithmetic means RQ values from the 48 µTOM measurements and the according standard deviation are in a 30% range of the arithmetic means RQ measured in the RAMOS device (Supporting Information 12). Consequently, the results from the RAMOS device as an independent reference method prove the accuracy of the novel CO_2 sensors in the µTOM.

4 | Conclusion

It was shown that a novel optical CO_2 sensor that relies on the dual lifetime referencing read-out scheme and is spectrally compatible to the optoelectronics of the µTOM device enables continuous monitoring the CO_2 partial pressure in individual wells of a 96-deepwell MTP. As sensor drift was observed, an appropriate online calibration method was developed. It allowed correct measurements of the CTR during microbial cultivations. The measurements obtained in the µTOM are in good agreement with parallel shake flask cultivations.

The novel sensor layout for the µTOM was used to monitor cultivations of *H. polymorpha* (*O. angusta*) and *E. coli*. The RQ monitoring allowed to characterize the predominant metabolism and the identification of the consumed carbon sources. The results show the potential of the µTOM device for the characterization of microbial cultivations in 96-deepwell MTP.

Considering quadruplicate cultivations, one reference condition and 23 new cultivation conditions, the OTR, CTR, and RQ can be monitored using the novel sensor layout. The RQ is calculated from simultaneous measurement of CTR and OTR in separate replicate wells. Hence, compared with the RAMOS system for eight shake flasks, the experimental throughput is increased by more than sevenfold.

Nomenclature

pCO_2	carbon dioxide partial pressure, [hPa]
n	shaking frequency, [rpm]
T	cultivation temperature, [K]
R	universal gas constant, [$L \cdot Pa \cdot mol^{-1} \cdot K^{-1}$]
YPG	yeast extract peptone glycerol medium, -
YPD	yeast extract peptone dextrose medium, -
w/v	weight per volume percent, [%]
vvm	volume flow per volume medium per minute, [SmL/mL/min]

TB	terrific broth, -
RAMOS	respiration activity monitoring system, -
µRAMOS	respiration activity monitoring system for 48-well microtiter plates, -
OTR_{max}	maximum oxygen transfer capacity, [mmol·L^{-1}·h^{-1}]
OTR	oxygen transfer rate, [mmol·L^{-1}·h^{-1}]
CTR	carbon dioxide transfer rate, [mmol·L^{-1}·h^{-1}]
RQ	respiratory quotient (CTR/OTR), [-]
OD_{600}	optical density (wavelength 600 nm), [A.U.]
$M_{Biomass}$	molar mass of biomass ($CH_2N_{0.25}O_{0.5}$), 21.51$\frac{g}{mol}$
$M_{Glucose}$	molar mass of glucose, 180$\frac{g}{mol}$
$M_{Glycerol}$	molar mass of glycerol, 92.1$\frac{g}{mol}$
MTP	microtiter plate, -
MFC	mass flow controller, -
d_0	shaking diameter, [mm]
µTOM	transfer rate online-monitoring device for 96-deepwell MTP, -
$\frac{dpCO_2}{dt}$	slope of the linearly increasing carbon dioxide partial pressure, [hPa·h^{-1}]
V_L	filling volume, [mL]
V_G	gas volume in the headspace of each well, [mL]
$\dot{V}$	controlled aeration flow, [SmL·min^{-1}]
$Y_{\frac{Biomass}{Glucose}}$	biomass yield for growth on glucose, [-]
$Y_{\frac{Biomass}{Glycerol}}$	biomass yield for growth on glycerol, [-]
$b_{0,0}$	initial calibration parameter of the CO_2-sensors, [-]
$a_{0,0}$	initial calibration parameter of the CO_2-sensors, [-]
$b_{1,0}$	initial calibration parameter of the CO_2-sensors, [-]
$a_{0,d}$	drift-compensated calibration parameter of the CO_2-sensors, [-]
$b_{0,d}$	drift-compensated calibration parameter of the CO_2-sensors, [-]
$b_{1,d}$	drift-compensated calibration parameter of the CO_2-sensors, [-]
$d\varphi_{air}$	phase shift in air, [°]
$d\varphi$	phase shift, [°]
$\frac{d\varphi}{d\varphi_{air}}$	relative sensor drift, [-]

Author Contributions

Robert Dinger designed this study, conducted the experiments, analyzed data, designed the measurement software, implemented the online calibration method, and drafted the manuscript. David Pfeifer prepared the new indicator dye for CO_2 measurements and optimized the composition of the sensing material. Clemens Lattermann constructed the measurement compartment and the sealing mechanism and critically revised the manuscript. David Flitsch developed the necessary drivers for the software and developed, manufactured the sensors, developed, and performed the calibration method and critically revised the manuscript. Jan P. Fischer developed and manufactured the 96-sensor module, devised the lifting mechanism. Sergey M. Borisov initiated and supervised the development of the CO_2 sensors, and critically revised the manuscript. Jochen Büchs initiated and supervised the study, participated in data interpretation, and critically revised the manuscript.

Acknowledgments

We are thankful for the financial support by the German Federal Ministry of Education and Research (BMBF, Grant number: 031B0102A). We thank the Institute for Molecular Enzyme Technology and the Institute for Microbiology at the Heinrich-Heine-University in Düsseldorf (Germany) for kindly providing the *E. coli* BL21(DE3) pRotHi-YFP and *H. polymorpha* RB11 pC10-FMD (P_{FMD}-GFP) strains, respectively. Open Access funding enabled and organized by Projekt DEAL.

Conflicts of Interest

David Flitsch and Jan P. Fischer were employees of the company PyroScience GmbH. These affiliations constitute no conflicts of interest with the results presented and discussed in this study. The remaining authors also declare no conflicts of interest.

References

Anderlei, T., and J. Büchs. 2001. "Device for Sterile Online Measurement of the Oxygen Transfer Rate in Shaking Flasks." *Biochemical Engineering Journal* 7, no. 2: 157–162. https://doi.org/10.1016/S1369-703X(00)00116-9.

Anderlei, T., W. Zang, M. Papaspyrou, and J. Büchs. 2004. "Online Respiration Activity Measurement (OTR, CTR, RQ) in Shake Flasks." *Biochemical Engineering Journal* 17, no. 3: 187–194. https://doi.org/10.1016/S1369-703X(03)00181-5.

Atkinson, B., and F. Mavituna. 1982. *Biochemical Engineering and Biotechnology Handbook*. Nature Press. https://www.osti.gov/biblio/5410841.

Ausubel, F. M., R. Brent, R. E. Kingston, et al. 1989. "Current Protocols in Molecular Biology, edited by M. Ausubel, R. Brent, R. E. Kingston, D. D. Moore, J. G. Seidman, J. A. Smith, and K. Struhl. Volumes 1 and 2. John Wiley & Sons, Inc., Media, PA, 1988, $165.00." *Molecular Reproduction and Development* 1, no. 2: 146. https://doi.org/10.1002/mrd.1080010210.

Borisov, S. M., K. Gatterer, B. Bitschnau, and I. Klimant. 2010. "Preparation and Characterization of Chromium(III)-Activated Yttrium Aluminum Borate: A New Thermographic Phosphor for Optical Sensing and Imaging at Ambient Temperatures." *Journal of Physical Chemistry C* 114, no. 19: 9118–9124. https://doi.org/10.1021/jp1016467.

Borisov, S. M., G. Nuss, and I. Klimant. 2008. "Red Light-Excitable Oxygen Sensing Materials Based on Platinum(II) and Palladium(II) Benzoporphyrins." *Analytical Chemistry* 80, no. 24: 9435–9442. https://doi.org/10.1021/ac801521v.

Borisov, S. M., C. Würth, U. Resch-Genger, and I. Klimant. 2013. "New Life of Ancient Pigments: Application in High-Performance Optical Sensing Materials." *Analytical Chemistry* 85, no. 19: 9371–9377. https://doi.org/10.1021/ac402275g.

Dinger, R., C. Lattermann, D. Flitsch, J. P. Fischer, U. Kosfeld, and J. Büchs. 2022. "Device for Respiration Activity Measurement Enables the Determination of Oxygen Transfer Rates of Microbial Cultures in Shaken 96-Deepwell Microtiter Plates." *Biotechnology and Bioengineering* 119, no. 3: 881–894. https://doi.org/10.1002/bit.28022.

Flitsch, D., S. Krabbe, T. Ladner, et al. 2016. "Respiration Activity Monitoring System for Any Individual Well of a 48-Well Microtiter Plate." *Journal of Biological Engineering* 10: 14. https://doi.org/10.1186/s13036-016-0034-3.

Forsten, E., S. Gerdes, R. Petri, J. Büchs, and J. Magnus. 2024. "Unraveling the Impact of pH, Sodium Concentration, and Medium Osmolality on *Vibrio natriegens* in Batch Processes." *BMC Biotechnology* 24, no. 1: 63. https://doi.org/10.1186/s12896-024-00897-8.

Fritzsche, E., P. Gruber, S. Schutting, et al. 2017. "Highly Sensitive Poisoning-Resistant Optical Carbon Dioxide Sensors for Environmental

Monitoring." *Analytical Methods* 9, no. 1: 55–65. https://doi.org/10.1039/C6AY02949C.

Gruber, P., M. P. C. Marques, N. Szita, and T. Mayr. 2017. "Integration and Application of Optical Chemical Sensors in Microbioreactors." *Lab on a Chip* 17, no. 16: 2693–2712. https://doi.org/10.1039/c7lc00538e.

Hemmerich, J., S. Noack, W. Wiechert, and M. Oldiges. 2018. "Microbioreactor Systems for Accelerated Bioprocess Development." *Biotechnology Journal* 13, no. 4: 1700141. https://doi.org/10.1002/biot.201700141.

Heyman, B., R. Lamm, H. Tulke, L. Regestein, and J. Büchs. 2019. "Shake Flask Methodology for Assessing the Influence of the Maximum Oxygen Transfer Capacity on 2,3-Butanediol Production." *Microbial Cell Factories* 18, no. 1: 78. https://doi.org/10.1186/s12934-019-1126-9.

Huber, C., I. Klimant, C. Krause, and O. S. Wolfbeis. 2001. "Dual Lifetime Referencing as Applied to a Chloride Optical Sensor." *Analytical Chemistry* 73, no. 9: 2097–2103. https://doi.org/10.1021/ac9914364.

Ihling, N., N. Bittner, S. Diederichs, et al. 2018. "Online Measurement of the Respiratory Activity in Shake Flasks Enables the Identification of Cultivation Phases and Patterns Indicating Recombinant Protein Production in Various *Escherichia coli* Host Strains." *Biotechnology Progress* 34, no. 2: 315–327. https://doi.org/10.1002/btpr.2600.

Ihling, N., L. P. Munkler, C. Berg, et al. 2021. "Time-Resolved Monitoring of the Oxygen Transfer Rate of Chinese Hamster Ovary Cells Provides Insights Into Culture Behavior in Shake Flasks." *Frontiers in Bioengineering and Biotechnology* 9: 725498. https://doi.org/10.3389/fbioe.2021.725498.

Kensy, F., E. Zang, C. Faulhammer, R. K. Tan, and J. Büchs. 2009. "Validation of a High-Throughput Fermentation System Based on Online Monitoring of Biomass and Fluorescence in Continuously Shaken Microtiter Plates." *Microbial Cell Factories* 8: 31. https://doi.org/10.1186/1475-2859-8-31.

Kopp, J., C. Slouka, S. Ulonska, et al. 2017. "Impact of Glycerol as Carbon Source Onto Specific Sugar and Inducer Uptake Rates and Inclusion Body Productivity in *E. coli* BL21(DE3)." *Bioengineering (Basel, Switzerland)* 5, no. 1: 1. https://doi.org/10.3390/bioengineering5010001.

Kunze, M., R. Huber, C. Gutjahr, S. Müllner, and J. Büchs. 2012. "Predictive Tool for Recombinant Protein Production in *Escherichia coli* Shake-Flask Cultures Using an On-Line Monitoring System." *Biotechnology Progress* 28, no. 1: 103–113. https://doi.org/10.1002/btpr.719.

Lippitsch, M. E., J. Pusterhofer, M. J. P. Leiner, and O. S. Wolfbeis. 1988. "Fibre-Optic Oxygen Sensor With the Fluorescence Decay Time as the Information Carrier." *Analytica Chimica Acta* 205: 1–6. https://doi.org/10.1016/S0003-2670(00)82310-7.

Liu, Y., Y. Tang, N. N. Barashkov, et al. 2010. "Fluorescent Chemosensor for Detection and Quantitation of Carbon Dioxide Gas." *Journal of the American Chemical Society* 132, no. 40: 13951–13953. https://doi.org/10.1021/ja103947j.

Lye, G. J., P. Ayazi-Shamlou, F. Baganz, P. A. Dalby, and J. M. Woodley. 2003. "Accelerated Design of Bioconversion Processes Using Automated Microscale Processing Techniques." *Trends in Biotechnology* 21, no. 1: 29–37. https://doi.org/10.1016/S0167-7799(02)00011-2.

Mills, A., and Q. Chang. 1993. "Fluorescence Plastic Thin-Film Sensor for Carbon Dioxide." *Analyst* 118, no. 7: 839. https://doi.org/10.1039/AN9931800839.

Müller, J., A. Hütterott, T. Habicher, N. Mußmann, and J. Büchs. 2019. "Validation of the Transferability of Membrane-Based Fed-Batch Shake Flask Cultivations to Stirred-Tank Reactor Using Three Different Protease Producing Bacillus Strains." *Journal of Bioscience and Bioengineering* 128, no. 5: 599–605. https://doi.org/10.1016/j.jbiosc.2019.05.003.

Müller, M. J., S. Stachurski, P. Stoffels, K. Schipper, M. Feldbrügge, and J. Büchs. 2018. "Online Evaluation of the Metabolic Activity of *Ustilago maydis* on (Poly)Galacturonic Acid." *Journal of Biological Engineering* 12: 34. https://doi.org/10.1186/s13036-018-0128-1.

Neuss, A., T. Steimann, J. S. Tomas Borges, R. Dinger, and J. B. Magnus. 2025. "Scale-Up of CHO Cell Cultures: From 96-Well-Microtiter Plates to Stirred Tank Reactors Across Three Orders of Magnitude." *Journal of Biological Engineering* 19, no. 1: 5. https://doi.org/10.1186/s13036-024-00475-8.

Pfeifer, D., I. Klimant, and S. M. Borisov. 2018. "Ultrabright Red-Emitting Photostable Perylene Bisimide Dyes: New Indicators for Ratiometric Sensing of High pH or Carbon Dioxide." *Chemistry (Weinheim an der Bergstrasse, Germany)* 24, no. 42: 10711–10720. https://doi.org/10.1002/chem.201800867.

Rahmen, N., A. Fulton, N. Ihling, M. Magni, K. E. Jaeger, and J. Büchs. 2015. "Exchange of Single Amino Acids at Different Positions of a Recombinant Protein Affects Metabolic Burden in *Escherichia coli*." *Microbial Cell Factories* 14: 10. https://doi.org/10.1186/s12934-015-0191-y.

Rahmen, N., C. D. Schlupp, H. Mitsunaga, et al. 2015. "A Particular Silent Codon Exchange in a Recombinant Gene Greatly Influences Host Cell Metabolic Activity." *Microbial Cell Factories* 14, no. 1: 156. https://doi.org/10.1186/s12934-015-0348-8.

Rappitsch, T., I. Klimant, and S. M. Borisov. 2020. "Bright Far-Red Emitting BODIPYs Via Extension With Conjugated Fluorene and Carbazole Motifs." *Dyes and Pigments* 174: 108037. https://doi.org/10.1016/j.dyepig.2019.108037.

Samorski, M., G. Müller-Newen, and J. Büchs. 2005. "Quasi-Continuous Combined Scattered Light and Fluorescence Measurements: A Novel Measurement Technique for Shaken Microtiter Plates." *Biotechnology and Bioengineering* 92, no. 1: 61–68. https://doi.org/10.1002/bit.20573.

Schulte, A., J. V. Schilling, J. Nolten, et al. 2018. "Parallel Online Determination of Ethylene Release Rate by Shaken Parsley Cell Cultures Using a Modified RAMOS Device." *BMC Plant Biology* 18, no. 1: 101. https://doi.org/10.1186/s12870-018-1305-6.

Schutting, S., S. M. Borisov, and I. Klimant. 2013. "Diketo-Pyrrolo-Pyrrole Dyes as New Colorimetric and Fluorescent pH Indicators for Optical Carbon Dioxide Sensors." *Analytical Chemistry* 85, no. 6: 3271–3279. https://doi.org/10.1021/ac303595v.

Schutting, S., T. Jokic, M. Strobl, S. M. Borisov, D. Beer, and I. Klimant. 2015. "Nir Optical Carbon Dioxide Sensors Based on Highly Photostable Dihydroxy-aza-BODIPY Dyes." *Journal of Materials Chemistry C* 3, no. 21: 5474–5483. https://doi.org/10.1039/C5TC00346F.

Schutting, S., I. Klimant, D. de Beer, and S. M. Borisov. 2014. "New Highly Fluorescent pH Indicator for Ratiometric RGB Imaging of pCO_2." *Methods and Applications in Fluorescence* 2, no. 2: 024001. https://doi.org/10.1088/2050-6120/2/2/024001.

Stockmann, C., M. Losen, U. Dahlems, C. Knocke, G. Gellissen, and J. Buchs. 2003. "Effect of Oxygen Supply on Passaging, Stabilising and Screening of Recombinant Production Strains in Test Tube Cultures." *FEMS Yeast Research* 4, no. 2: 195–205. https://doi.org/10.1016/S1567-1356(03)00147-8.

Stöckmann, C., U. Maier, T. Anderlei, C. Knocke, G. Gellissen, and J. Büchs. 2003. "The Oxygen Transfer Rate as Key Parameter for the Characterization of *Hansenula polymorpha* Screening Cultures." *Journal of Industrial Microbiology & Biotechnology* 30, no. 10: 613–622. https://doi.org/10.1007/s10295-003-0090-9.

Teworte, S., K. Malcı, L. E. Walls, M. Halim, and L. Rios-Solis. 2022. "Recent Advances in Fed-Batch Microscale Bioreactor Design." *Biotechnology Advances* 55: 107888. https://doi.org/10.1016/j.biotechadv.2021.107888.

Wilms, B., A. Hauck, M. Reuss, et al. 2001. "High-Cell-Density Fermentation for Production of L-N-Carbamoylase Using an Expression

System Based on the Escherichia Coli rhaBAD Promoter." *Biotechnology and Bioengineering* 73: 95–103. https://doi.org/10.1002/bit.1041.

Supporting Information

Additional supporting information can be found online in the Supporting Information section.

Supporting information 1: Synthesis of the new indicator dye. 3,6-Bis[4′-bis(2-ethylhexyl)- sulfonylamide-1,1′-biphenyl-4-yl]-2,5-dihydropyrrolo- [3,4-c]pyrrole-1,4-dione (1) was synthesized according to literature procedure (Schutting et al., 2013). 100 mg (0.095 mmol) of 1 were dissolved in 10 mL of anhydrous dimethylformamide, 225 mg (1.6 mmol) of fine-powdered potassium carbonate were added and the dispersion was warmed to 60°C under stirring. After a color change from orange to blue, 20 µl (0.11 mmol) of 4-tert-butylbenzylbromide were added and the dispersion was stirred at 60°C for another 3 h. The mixture was cooled to room temperature and 5 mL of 1 M aqueous hydrochloric acid were added. After addition of water and dichloromethane the product was extracted into the organic phase and this was repeated three times. The organic phase was dried over anhydrous sodium sulfate and the solvents were evaporated under reduced pressure. The crude product was purified via column chromatography with silica-gel as stationary phase and dichloromethane/methanol (99/1 v/v) as an eluent to yield a dark red powder (29 mg, 25% yield). 1H NMR (300 MHz, CDCl3) δ 8.46 (s, 1H), 8.38 (d, J = 8.1 Hz, 2H), 7.94 – 7.83 (m, 6H), 7.80 – 7.66 (m, 8H), 7.36 (d, J = 8.0 Hz, 2H), 7.18 (d, J = 8.0 Hz, 2H), 5.06 (s, 2H), 3.12 – 2.85 (m, 8H), 1.72 – 0.77 (m, 69H). MS (MALDI-TOF): m/z [MH]+ 1193.7072 (found), 1193.7163 (calc.); [M+Na]+ 1215.6858 (found), 1215.6962 (calc.).

Supporting information 2: Mass spectrum (MALDI-TOF) of the indicator 2.

Supporting information 3: 1H NMR (300 MHz, CDCl3) of indicator 2.

Supporting information 4: Left: Absorption (solid lines) and fluorescence (pointed lines) spectra of indicator 2 in toluene solution in the neutral form (black lines) and deprotonated form (addition of tetraoctylammonium hydroxide, red lines). Right: Excitation and emission spectra of Egyptian blue in form of microcrystalline powder.

Supporting information 5: Sensing principle of the CO2 sensor. In the absence of carbon dioxide the indicator 2 is in its deprotonated form due to the presence of tetraoctylammonium base. Protonation of the indicator in presence of carbon dioxide results in hypsochromic shift of absorption and emission bands (Supporting information 4) and thus in decrease of fluorescence intensity upon excitation with the red light. Both the indicator and the lipophilic base are embedded into ethylcellulose polymeric matrix.

Supporting information 6: Cross-sectional drawing of two of the 96 measuring positions (wells) within the µTOM device during the flow and the stop phase. During the flow phase, the microtiter plate (MTP) is lowered (blue arrow, downwards), allowing ventilation of the wells with a defined total air flow $\dot{V}$. In the stop phase, the MTP is lifted and pressed against the sealing layer (Figure 1 A, 9). Consequently, all wells are gas-tightly sealed and, thereby, the ventilation of the wells is stopped.

Supporting information 7: Side view of the setup used for calibration, without the optional gas washing bottle shown in Figure 3 e.

Supporting information 8: Schematic depiction of necessary calibration steps, to allow accurate pCO2-measurements by sensor drift compensation. The initial 7-point calibration (Figure 4) and drift characterization (Figure 5) are performed in the calibration setup (Figure 3 and Supporting Information 7) for every produced sensor batch, as illustrated in Figure. The seven point calibration yields the initial calibration parameters $a_{0,0}$, $b_{0,0}$ and $b_{1,0}$ of the sensor batch. The drift characterization allows to calculate the drift compensated calibration parameters $\mathbf{b_{0,d}}$, $\mathbf{b_{1,d}}$ as functions of their initial values ($b_{0,0}$ and $b_{1,0}$) and the relative sensor drift $\frac{d\varphi_{\text{air}}}{d\varphi_{air,0}}$. The relative sensor drift is determined as a one point calibration before each stop phase (Figure 2, Cn) during cultivations. Subsequently, the drift compensated calibration parameter $a_{0,d}$ is optimized (downhill-simplex) to fit Equation 3 to the online one-point calibration in air (Figure 2, Cn) and to allow the drift compensated calculation of the pCO_2.

Supporting Information 9: Determination of the calibration parameter $a_{0,d}$ during the exposure of the CO2 sensor in air containing traces of acetic acid, as shown in Figure 5 A. The refitted parameter $a_{0,d}$ normalized to the initial parameter a_0 values at 0 h of exposure of four CO2 sensors are shown in dependence on the current phase shift in air ($d\varphi_{air,d}$) normalized with the phase shift in air at 0 h of exposure to acetic acid ($d\varphi_{air,0}$). A linear fit for the calibration parameter $\frac{a_{0,d}}{a_{0,0}}$ was calculated and is depicted as a black dashed line.

Supporting information 10: Empirical correlation for the OTRmax (Dinger et al., 2022), depending on the filling volume (VL [mL]), shaking diameter (d0 [mm]) and shaking frequency (n [rpm]). The presented correlation is used to predict the OTRmax in 96-deepwell MTP with a round cross-section (well diameter = 7 mm), when filled with Newtonian fluids with viscosities similar to that of water.

Supporting Information 11: Degree of reduction.

Supporting Information 12: Respiration quotient of parallel cultivations of E. coli BL21(DE3) pRotHi-YFP in the µTOM device (—▼—) and the RAMOS device (—■—) depicted in Figure 7. The data points represent the arithmetic mean values (RAMOS N = 7, µTOM N = 48). The red shadow marks a 30% confidence interval around the arithmetic mean values from the RAMOS device. The blue shadow depicts the standard deviation of 48 replicate RQ measurements in the µTOM device.

Supporting Information 13: The sensor layout in the lid of the µTOM device is depicted. The oxygen partial pressure is measured in all wells in rows A to D of the microtiter plate. In all wells of rows E to H the carbon dioxide partial pressure is measured. Replicate cultivations are performed according to the well paring for RQ calculations. For example, the first RQ value is calculated from the CTR measured in well E1 divided by the OTR measured in well A1 $\left(RQ_1 = \frac{CTR_{E1}}{OTR_{A1}}\right)$. By this pairing in total 48 RQ values can be calculated for 48 duplicate cultivations.